Quantum corrections to solitons in the ϕ^8 model

I. Takyi[●],[1] M. K. Matfunjwa[●],[2,3] and H. Weigel[●][4]

[1]*Mathematics Department, Kwame Nkrumah University of Science and Technology,*
Private Mail Bag, University Post Office, KNUST-Kumasi, Ghana
[2]*African Institute for Mathematical Sciences, 6 Melrose Road, Muizenberg, 7945 Cape Town, South Africa*
[3]*Department of Physics, University of Eswatini, Private Bag 4, Kwaluseni M201, Eswatini*
[4]*Institute for Theoretical Physics, Physics Department, Stellenbosch University,*
Matieland 7602, South Africa

We compute the vacuum polarization energy of kink solitons in the ϕ^8 model in one space and one time dimensions. There are three possible field potentials that have eight powers of ϕ and that possess kink solitons. For these different field potentials we investigate whether the vacuum polarization destabilizes the solitons. This may particularly be the case for those potentials that have degenerate ground states with different curvatures in field space yielding different thresholds for the quantum fluctuations about the solitons at negative and positive spatial infinity. We find that destabilization occurs in some cases, but this is not purely a matter of the field potential but also depends on the realized soliton solution for that potential. One of the possible field potentials has solitons with different topological charges. In that case the classical mass approximately scales like the topological charge. Even though destabilization precludes robust statements, there are indications that the vacuum polarization energy does not scale as the topological charge.

I. INTRODUCTION

Solitons are stable, localized particlelike solutions to nonlinear wave equations in field theories [1–3]. These particlelike solutions include solitons such as monopoles in $(3 + 1)$ dimensions and vortices, strings and lumps in $(2 + 1)$ dimensions. The soliton solutions have wide applications in many branches of physics: in cosmology [4], condensed matter physics [5,6], as well as hadron and nuclear physics [7]. The interested reader is directed to those textbooks and review articles for more details and further references.

In one space and one time dimensional models with distinct vacua, soliton solutions connect neighboring vacua between negative and positive spatial infinity. As there is no finite energy continuous transformation between these vacua at spatial infinity, these so-called kink solitons are topologically stable. When embedded in higher dimensions, these kinks emerge as branes or interfaces. In one space dimension dynamical stability can be argued for from Derrick's theorem [8]. The derivative and potential contributions to the classical energy scale oppositely when

varying the extension of the kink. The derivative part diverges when the static configuration is shrunk to a point, so does the potential part for wide configurations. Hence the classical energy is minimized for a finite size of the kink. The situation may, however, change when nonlocal quantum effects are included. Here we will therefore compute the leading (one-loop) quantum correction to the classical energy of the kink using spectral methods [9]. Such corrections have also been computed within the heat kernel expansion with ζ-function regularization [10,11] for other soliton models. Agreement is observed whenever comparison is possible. However, spectral methods are technically less involved and do not require the truncation of an expansion.

Generally nonlinear field theories have degenerate vacua with different curvatures in field space. The different curvatures translate into different masses for the fluctuations about the degenerate vacua. We will call *primary* vacuum the one with the lowest of all allowed masses, the others will be called *secondary* vacua. In models with several fields the primary vacuum contains the smallest of all curvature eigenvalues. It has recently been conjectured that the occurrence of such secondary vacua causes the solitons to be unstable on the quantum level. As the kink occupies the secondary vacuum over an increasing region in space, the one-loop quantum energy decreases without a lower bound and thereby destabilizes the kink.

This conjecture has been drawn from two model calculations, in the ϕ^6 model [12,13] and the multifield Shifman-Voloshin model [14,15]. In the context of the ϕ^6 model, a similar conclusion was drawn when it was observed that fluctuations produce a net force on the kink [16].

In this paper we will consider the ϕ^8 model that also contains topologically stable solitons [17,18] and which, for certain model parameters, exhibits secondary vacua. Recently this model has attracted quite some attention, cf. Ref. [19] and references therein, as it induces long range interactions in the kink-antikink scattering. In this model we will find that indeed the vacuum polarization energy (VPE), which is the leading quantum correction to the soliton static energy, is not bounded from below in certain versions of this model either. We note that though the ϕ^8 is superrenormalizable (as any scalar theory in one space and one time dimensions) perturbatively, we will see that renormalizability is nevertheless an issue and that only a particular renormalization condition (the no-tadpole prescription) leads to a finite quantum correction. Super-renormalizability makes statements on the number the divergent Feynman diagrams but not the structure of the counterterms.

In the next section we briefly outline the construction principle of soliton solutions in one (space) dimensional models and list the field potentials for our present study. In Sec. III we describe the general formalism for computing the one-loop energy correction to the energies of the solitons that we construct explicitly in Sec. IV. We present and discuss our numerical results in Sec. V and conclude in Sec. VI.

II. THE MODELS

Starting point is the general Lagrangian for a $D = 1 + 1$ dimensional model

$$\mathcal{L} = \frac{1}{2}\partial_\mu\phi\partial^\mu\phi - U(\phi), \qquad (1)$$

where $U(\phi)$ is the field potential that governs the dynamics. In one space dimension it is standard to derive a first order differential equation for the soliton profile [1]. Integrating the right-hand side in

$$x - x_0 = \pm \int_{\phi_K(x_0)}^{\phi_K(x)} \frac{d\phi}{\sqrt{2U(\phi)}} \qquad (2)$$

then yields an implicit function for the profile function $\phi_K(x)$. The first order formalism furthermore simplifies the classical energy (mass)

$$E_{\text{cl}} = M = \int_{-\infty}^{\infty} dx \left[\frac{1}{2}\left(\frac{d\phi_K}{dx}\right)^2 + U(\phi_K) \right]$$

$$= \int_{\phi_K(-\infty)}^{\phi_K(\infty)} d\phi \sqrt{2U(\phi)} \qquad (3)$$

for the soliton solution. For the ϕ^8 model we consider three different field potentials

$$U_2(\phi) = \lambda^2(\phi^2 - a^2)^2(\phi^2 + b^2)^2,$$
$$U_3(\phi) = \lambda^2(\phi^2 - a^2)^2(\phi^2 + b^2)\phi^2 \quad \text{and}$$
$$U_4(\phi) = \lambda^2(\phi^2 - a^2)^2(\phi^2 - b^2)^2. \qquad (4)$$

The subscripts denote the number of degenerate vacua that the respective potential contains.

Before discussing the model and its soliton solutions in more detail we will briefly review the computation of the VPE, in particular in the context that secondary vacua exist.

III. VACUUM POLARIZATION ENERGY

The VPE, E_{vac} emerges from the shift of the zero point energies of the fluctuations in the presence of the soliton. This shift manifests itself in two contributions, from the discrete bound states (b.s.) and from the modified density of the scattering states $\Delta\rho(k)$. Here k is the wave number of the continuous scattering states. We thus write

$$E_{\text{vac}} = \frac{1}{2}\sum_j^{\text{b.s.}} E_j + \frac{1}{2}\int_0^\infty dk \sqrt{k^2 + m_L^2}\,\Delta\rho(k) + E_{\text{ct}}, \qquad (5)$$

where m_L is the mass for fluctuations about the primary vacuum and E_{ct} is the contribution from the counterterms that render the model finite at one-loop order. We extract both the bound state energies E_j and $\Delta\rho(k)$ from the fluctuations $\eta(t, x)$ about the soliton. Since the soliton is static we can separate the time dependence as $\eta(t, x) = e^{i\omega t}\eta(x)$. We then linearize the field equations for a general field potential $U(\phi)$:

$$\left[-\frac{d^2}{dx^2} + V(x) \right]\eta(x) = \omega^2\eta(x), \quad \text{where}$$

$$V(x) = \frac{d^2U(\phi)}{d\phi^2}\bigg|_{\phi=\phi_K(x)}. \qquad (6)$$

As described at the end of this section, it is straightforward to (numerically) obtain the discrete b.s. solutions $\omega = E_j$ with $0 \leq E_j \leq m_L$. The continuous scattering states are parametrized by real $k = \sqrt{\omega^2 - m_L^2}$. Unfortunately, extracting scattering data and subsequently $\Delta\rho(k)$ is subtle when there are secondary vacua. In such a case the background potential $V(x)$ approaches different values at negative and positive spatial infinity. We take our frame of reference such that $\lim_{x\to-\infty}V(x) = m_L^2$ and define $m_R^2 = \lim_{x\to+\infty}V(x)$ so that always $m_R \geq m_L$.

According to the Krein formula [20] we find that

$$\Delta\rho(k) = \frac{1}{\pi}\frac{d\delta(k)}{dk} \quad \text{where} \quad \delta(k) = -\frac{i}{2}\log\left[\det S(k)\right] \quad (7)$$

is the sum of the eigenphase shifts that we extract from the scattering matrix[1] $S(k)$. To compute $S(k)$ we first define the pseudopotential

$$V_p(x) = V(x) - m_L^2 + (m_L^2 + m_R^2)\Theta(x - x_m), \quad (8)$$

where x_m is an arbitrary matching point. Then the wave equation reads

$$\left[-\frac{d^2}{dx^2} + V_p(x)\right]\eta(x) = \begin{cases} k^2\eta(x), & x \leq x_m, \\ q^2\eta(x), & x \geq x_m, \end{cases} \quad (9)$$

with $q = \sqrt{k^2 + m_L^2 - m_R^2}$. For real q, i.e., $k \geq \sqrt{m_R^2 - m_L^2}$ we formulate a variable phase approach [21] by parametrizing

$$x \leq x_m: \ \eta(x) = A(x)e^{ikx}$$
$$A''(x) = -2ikA'(x) + V_p(x)A(x)$$
$$x \geq x_m: \ \eta(x) = B(x)e^{iqx}$$
$$B''(x) = -2iqB'(x) + V_p(x)B(x). \quad (10)$$

Here, and subsequently, a prime denotes the derivative with respect to the coordinate x. We solve Eq. (10) with boundary conditions $A(-\infty) = B(\infty) = 1$ and $A'(-\infty) = B'(\infty) = 0$ yielding the scattering matrix [22]

$$S(k) = \begin{pmatrix} e^{-iqx_m} & 0 \\ 0 & e^{ikx_m} \end{pmatrix}\begin{pmatrix} B & -A^* \\ iqB + B' & ikA^* - A'^* \end{pmatrix}^{-1}$$
$$\times \begin{pmatrix} A & -B^* \\ ikA + A' & iqB^* - B'^* \end{pmatrix}\begin{pmatrix} e^{ikx_m} & 0 \\ 0 & e^{-iqx_m} \end{pmatrix}, \quad (11)$$

where $A = A(x_m)$, etc., are the coefficient functions at the matching point. In the second case, $k \leq \sqrt{m_R^2 - m_L^2}$ we replace iq by $\kappa = \sqrt{m_R^2 - m_L^2 - k^2} \geq 0$ and parametrize the wave function for $x \geq x_m$ as $\eta(x) = B(x)e^{-\kappa x}$. In that region the differential equation now reads $B''(x) = \kappa B'(x) + V_p(x)B$ and we extract the reflection coefficient as

$$S(k) = -\frac{A(B'/B - \kappa - ik) - A'}{A^*(B'/B - \kappa + ik) - A'^*}e^{2ikx_m}. \quad (12)$$

In the nontadpole renormalization scheme, which is the only one applicable when secondary vacua emerge [12],

the counterterm contribution in Eq. (5) subtracts exactly the Born approximation $\delta^{(1)}$ from the phase shift [9]. Again there is subtlety in the presence of secondary vacua as there is a direct contribution from the pseudopotential as well as from the step function potential inherited from the different masses

$$\delta^{(1)}(k) = -\frac{1}{2k}\int_{-\infty}^{\infty} dxV_p(x)\bigg|_{x_m} + \frac{x_m}{2k}(m_R^2 - m_L^2)$$
$$= -\frac{1}{2k}\int_{-\infty}^{\infty} dxV_p(x)\bigg|_0. \quad (13)$$

Here the subscript gives the position of the step in the pseudopotential, $V_p(x)$. We stress that this Born approximation for the phase shift is obtained from the full fluctuation potential, $V(x) - m_L^2$. In Eq. (8) we used the unique feature that the Born approximation is linear in the fluctuation potential to obtain a well-defined integral representation. Especially we have thus found that a particular matching point must be chosen and that there is no variation of the Born approximation with x_m. Of course, for numerical evaluations we always verify that this is the case for the full calculation. In total, the vacuum polarization is computed as
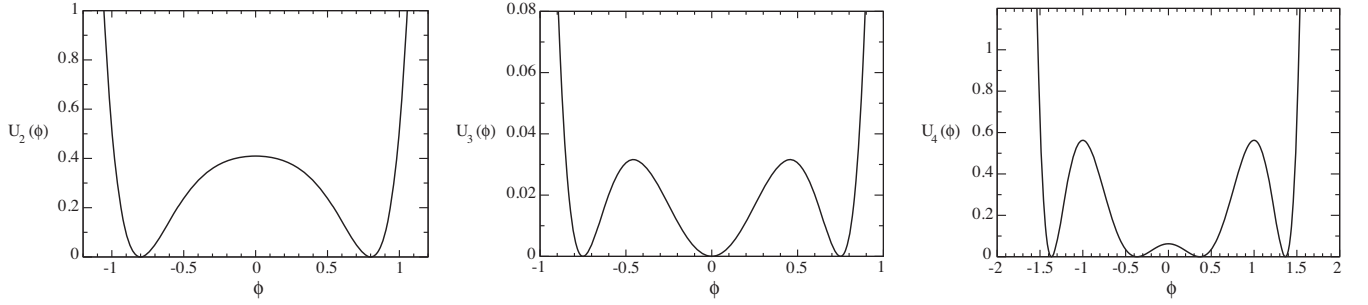
$$E_{\text{vac}} = \frac{1}{2}\sum_j (E_j - m_L)$$
$$- \frac{1}{2\pi}\int_0^\infty dk\frac{k}{\sqrt{k^2 + m_L^2}}(\delta(k) - \delta^{(1)}(k)). \quad (14)$$

In the introduction we mentioned that the renormalization of the VPE in the ϕ^8 model would only be possible for the no-tadpole condition with respect to the full potential. This is exactly what Eq. (14) implies. There is no leftover first order contribution to the VPE. Any first order finite renormalization would contain an integral of the full fluctuation potential. It cannot be the pseudopotential since the model by itself has no information on the matching point. However, the integral over the full fluctuation potential does not exist when $m_R \neq m_L$.

For symmetric background potentials $V(-x) = V(x)$ (which implies $m_R = m_L$ and no secondary vacuum) a simpler formalism to compute the VPE exists. It makes ample use of analytic properties of scattering data and results in [9]

$$E_{\text{vac}}^S = \int_{m_L}^\infty \frac{dt}{2\pi}\frac{t}{\sqrt{t^2 - m_L^2}}$$
$$\times \left[\ln\left\{g(0,t)\left(g(0,t) - \frac{1}{t}g'(0,t)\right)\right\}\right]_1. \quad (15)$$

The subscript indicates that the Born approximation has been subtracted. Here $g(x,t)$ is the Jost solution factor that solves the differential equation

---

[1]Branches of the logarithm must be taken such that $\delta(k)$ is a smooth function with $\delta(\infty) = 0$.

FIG. 1.   Field potentials in the ϕ^8 model. From left to right for two, three and four degenerate vacua.

$$g''(x,t) = 2tg'(x,t) + V(x)g(x,t) \qquad (16)$$

for imaginary momenta $t = ik$ with boundary conditions $g(\infty, t) = 1$ and $g'(\infty, t) = 0$. We will use this formalism to verify our results in case $V(x)$ is indeed symmetric. It can also be used to consider $V(x_0 + x) + V(x_0 - x)$ [12]. For sufficiently large x_0 this is a noninterfering superposition and the resulting VPE is twice that of $V(x)$ [23]. Unfortunately, numerically there are restrictions on how large x_0 can be taken.

The wave equation (6) is also used to determine the bound state energies $E_j < m_L$. We integrate this equation with the initial conditions

$$\eta_L \to 1 \quad \text{and} \quad \eta_L' \to \sqrt{m_L^2 - E^2} \quad \text{for } x \to -\infty,$$

as well as

$$\eta_R \to 1 \quad \text{and} \quad \eta_R' \to -\sqrt{m_R^2 - m_L^2 - E^2} \quad \text{for } x \to \infty$$

from either side. Whenever we tune the energy to $E = E_j$ such that the Wronskian $\eta_L \eta_R' - \eta_R \eta_L'$ is zero at any intermediate coordinate (preferable x_m) we have identified a bound state energy.

IV. THE ϕ^8 SOLITONS

In this section we discuss the classical solutions from the field potentials in Eq. (4) and list the formulas for the resulting background potentials for the fluctuations. To a major part this discussion is a brief review of the findings from Ref. [18] with a particular emphasis on the vacuum structures and the implications for the fluctuations $\eta(t,x)$. Exemplary graphs for the field potentials in the three different sectors are shown in Fig. 1.

A. Two degenerate minima: U_2

For the case of $U = U_2$ the kink solution interpolating between $-a$ and a is given implicitly by

$$\pm m_R(x - x_0) = \frac{2a}{b} \arctan\left(\frac{\phi_K}{b}\right) + \ln\left(\frac{a + \phi_K}{a - \phi_K}\right), \quad (17)$$

where $m_R = \sqrt{8}\lambda a(a^2 + b^2)$. The corresponding classical kink mass is

$$M_{(-a,a)} = \frac{4\sqrt{2}}{15} \lambda a^3 (a^2 + 5b^2). \qquad (18)$$

The background potential for the fluctuations is symmetric under the spatial reflection $x \to -x$

$$
\begin{aligned}
V(x) &= V_2(x) \\
&= \lambda^2 \{ 56\phi_K^6 + 60(b^2 - 2a^2)\phi_K^4 \\
&\quad + 12(a^4 - 4a^2 b^2 + b^4)\phi_K^2 + 4a^4 b^2 - 4a^2 b^4 \}.
\end{aligned}
\tag{19}
$$

An example is shown in the top left panel of Fig. 2. By construction U_2 only has a primary vacua yielding $m_L = m_R$.

B. Three degenerate minima: U_3

When $U = U_3$ there are solitons that interpolate between the degenerate vacua at $\phi = a$ and $\phi = 0$. The implicit solution to the first order equation (2) with the boundary conditions $\phi \to 0$ as $x \to -\infty$ and $\phi \to a$ as $x \to \infty$ is

$$
e^{m_R(x-x_0)} = \left(\frac{\sqrt{b^2 + \phi_K^2} - b}{\sqrt{b^2 + \phi_K^2} + b}\right)^{\frac{\sqrt{b^2 + a^2}}{b}} \\
\times \left(\frac{\sqrt{b^2 + a^2} + \sqrt{b^2 + \phi_K^2}}{\sqrt{b^2 + a^2} - \sqrt{b^2 + \phi_K^2}}\right), \quad (20)
$$

with $m_R = 2\sqrt{2}\lambda a^2 \sqrt{a^2 + b^2}$. The resulting classical mass is

$$M_{(0,a)} = \frac{\sqrt{2}}{15} \lambda (2(b^2 + a^2)^{\frac{5}{2}} - b^3(2b^2 + 5a^2)). \qquad (21)$$
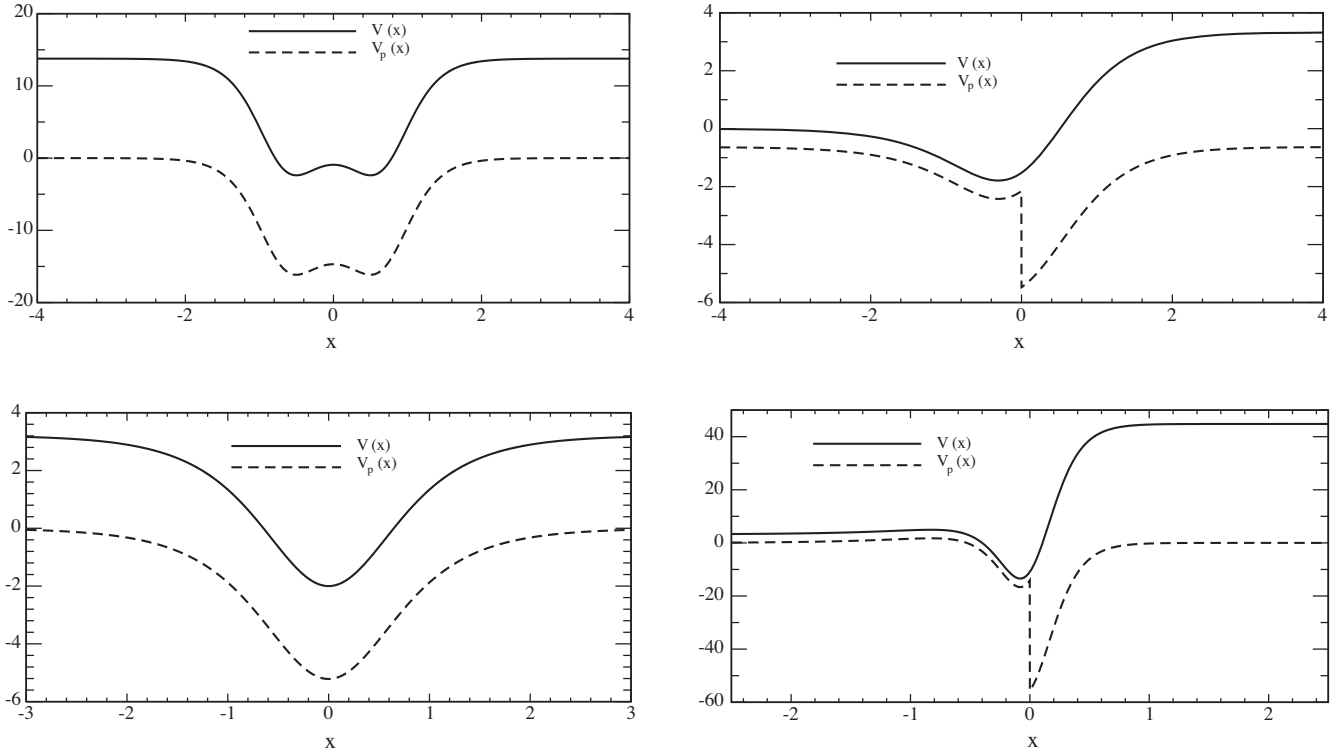
FIG. 2. Background- and pseudopotentials from solitons in the various sectors. All cases have $x_0 = 0$. Top row: models with two (left panel) and three (right panel) degenerate minima. Bottom row: model with four degenerate minima and symmetric (left panel) and nonsymmetric (right panel) solitons.

The background potential

$$V(x) = V_2(x)$$
$$= \lambda^2 \{56\phi_K^6 + 30(b^2 - 2a^2)\phi_K^4$$
$$+ 12(a^4 - 2a^2b^2)\phi_K^2 + 2a^4b^2\} \quad (22)$$

is not symmetric under the reflection $x \leftrightarrow -x$, cf. top right entry of Fig. 2. Consequently $V(-\infty) \neq V(\infty)$ and $m_L = \sqrt{2}\lambda a^2 b < m_R$. The field potential U_3 also has topologically equivalent solitons that interpolate between $\phi = -a$ and $\phi = 0$. We will not consider them here as they are not subject to our choice $m_L \leq m_R$. Of course, the numerical results coincide with those for the chosen soliton.

We note an interesting relation between the U_2 and U_3 models. In the limit $b \to 0$ the soliton of the U_2 model separates into two structures. In one region the soliton has a kink shape that connects $\phi = -a$ and $\phi \approx 0$. In the second region the soliton then connects $\phi \approx 0$ and $\phi = +a$. The smaller b, the further apart are these regions. Each of the two structures then is similar to a soliton of the U_3 model. Stated otherwise, any peculiar feature of the U_3 model (like instabilities) should also be seen in the U_2 model when the limit $b \to 0$ is considered.

C. Four degenerate minima: U_4

For the model with four degenerate minima, U_4 in Eq. (4) we take $b > a > 0$. The four degenerate minima

are at $\phi(x, t) = \pm a$ and $\phi(x, t) = \pm b$. The interesting feature is that there are two distinct soliton solutions with inequivalent topology.

1. Kink interpolating between $-a$ and $+a$

In this sector, the field is constrained to be $|\phi| < a$. The implicit solution for the kink is

$$e^{\pm m_L(x-x_0)} = \left(\frac{a + \phi_K}{a - \phi_K}\right)\left(\frac{b - \phi_K}{b + \phi_K}\right)^{\frac{a}{b}}, \quad (23)$$

where $m_L = \sqrt{8}\lambda a(b^2 - a^2)$. It has the classical mass

$$M_{(-a,a)} = \frac{4\sqrt{2}}{15}\lambda a^3(5b^2 - a^2). \quad (24)$$

The background potential for the fluctuations

$$V(x) = V_4(x)$$
$$= \lambda^2 \{56\phi_K^6 - 60(a^2 + b^2)\phi_K^4$$
$$+ 12(a^4 + 4a^2b^2 + b^4)\phi_K^2 - 4a^4b^2 - 4a^2b^4\} \quad (25)$$

is symmetric under the spatial reflection $x \leftrightarrow -x$. This, of course, implies $m_R = m_L$. A typical example is shown in the bottom left panel of Fig. 2.

2. Kink interpolating between a and b
(or −b and −a)

In this case the field is constrained by $a < |\phi| < b$ and the implicit solutions reads

$$e^{\pm m_L(x-x_0)} = \left(\frac{\phi_K - a}{\phi_K + a}\right)\left(\frac{b + \phi_K}{b - \phi_K}\right)^{\frac{a}{b}}, \qquad (26)$$

with m_L as above. For the kink in this sector the classical mass of the kink is

$$M_{(a,b)} = \frac{\sqrt{8}}{15}\lambda(b-a)^3(a^2 + 3ab + b^2). \qquad (27)$$

Formally and by construction, the background potential for the fluctuations is that of Eq. (25). However, since the kink is not invariant under spatial reflection, the background potential is not either and we obtain different mass parameters: $m_R = bm_L/a > m_L$.

V. NUMERICAL RESULTS

In this section we present the numerical results for the VPEs for the different topological sectors discussed above. As mention earlier, we take the model parameter $\lambda = 1$. This is legitimate as long as we are only interested in the VPE. In general, λ serves as a loop-counting parameter and the classical mass scales inversely with λ while the VPE is only proportional to m, where m is a mass parameter[2] in the potential $U(\phi)$.

We first note that for the classical soliton and the discrete bound state energies we have reproduced all numerical results reported in Ref. [18]. Of course, scattering solutions were not considered in that paper. When computing the phase shifts we have furthermore verified that the number of bound states n_{bs} agrees with Levinson's theorem in one space dimension [24,25] according to which the phase shift at zero momentum is $\delta(0) = \pi(n_{bs} - 1/2)$. Numerically there actually is a nontrivial ingredient as the phase shift computed from Eq. (7) is always between $-\pi/2$ and $+\pi/2$ with jumps of π whenever the determinant of the scattering matrix passes negative one. These jumps are eliminated by adding appropriate multiples of π to the phase shift with the boundary condition $\delta(\infty) = 0$. In this way we not only get a continuous phase shift, but also agreement with Levinson's theorem in all our simulations.

The computation of scattering data is hampered by the fact that the soliton profiles are only available in form of implicit expressions, cf. Eq. (17). Numerically we solve them by the method of nested intervals. Though that procedure is sufficiently efficient for quantities on the classical level, the differential equations of the scattering problem, Eqs. (9) and (10), are treated within an adaptive step size algorithm and *a priori* it is unknown at which coordinate the profile functions are needed. Therefore the nested intervals procedure must be applied at every coordinate requested by the algorithm. This is numerically time consuming.

In Fig. 2 we show examples for the background potential that enter the differential equations for the scattering data.

A. Two degenerate minima: U_2

The model with two degenerate minima of the field potential is conceptually that of the standard ϕ^4 kink model as the two vacua have equal curvature. Hence, as a proof of concept, we only compute the VPE for a single set of parameters that we take as in Ref. [18]: $a = \frac{4}{5}$ and $b = 1$. This translates into $m_L = m_R = 3.710$. The major interesting aspect is that there four bound states. Accordingly the phase shift at zero momentum approaches $7\pi/2$ as seen in the top left entry of Fig. 3. The bound state energies as well as the various contributions to the VPE and the VPE itself are listed in Table I. As for the standard kink, the leading quantum correction is negative. We have confirmed the VPE result using the Jost function formalism of Eq. (15). The numerical result from that calculation is $E_{vac}^S = -1.574$.

B. Three degenerate minima: U_3

Again we adopt the model parameters of Ref. [18]: $a = \frac{3}{4}$ and $b = 1$. Even though the model produces the translational zero mode as the only bound state, this model is nevertheless more interesting than the one with two degenerate minima. The reason is that with the additional minimum we now have primary and secondary vacua. This is most obvious from the meson masses (curvatures): $m_L = 0.7955$ and $m_R = 1.9887$. This yields -0.398 for the bound state contribution to the VPE irrespective of x_0. Furthermore, the phase shift exhibits the typical threshold cusp at $k = \sqrt{m_R^2 - m_L^2}$ as seen on the top right in Fig. 3. Obviously the phase shift at zero momentum, $\delta(0) \approx \pi/2$ is consistent with Levinson's theorem.

Most importantly the appearance of the secondary vacuum at spatial infinity induces a translational variance of the VPE as seen in Table II. As the kink is shifted towards the primary vacuum, the region with the secondary vacuum increases and low-lying modes disappear. Consequently the VPE decreases. As matter of fact, there is no bound to this decrease and the VPE can take any arbitrarily large negative value. Hence for any fixed loop-counting parameter λ, there will be an x_0 such that the total

---

[2]For this to be correct, the dimensionless parameters a and b must be written as $a = \alpha\sqrt[3]{m/\lambda}$ and $b = \beta\sqrt[3]{m/\lambda}$ where α and β do not vary with m or λ. With this scaling the quadratic mass type term in $U(\phi)$ does not contain the coupling constant λ. In turn the kink profile, ϕ_K also scales like $\sqrt[3]{m/\lambda}$ and the prefactor λ^2 cancels in $V(x)$, cf. Eq. (25). Then the classical mass scales as $(m/\lambda)^{2/3}$.
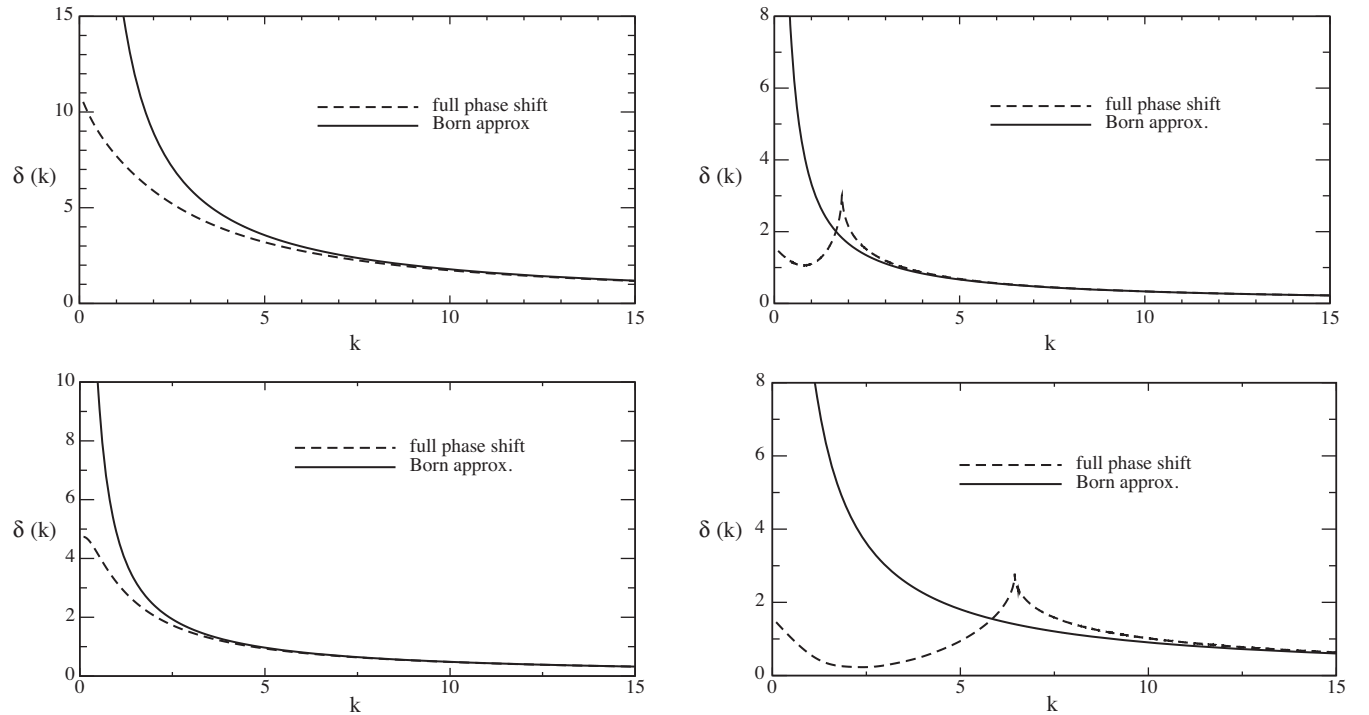
FIG. 3. Sample phase shifts in the various version of the ϕ^8 model. Top row: two (left) and three (right) degenerated vacua. Bottom row: four degenerate vacua for the sectors (a, a) and (a, b) in the left and right panels, respectively. The Born approximations are computed from Eq. (13).

energy is negative and the quantum corrections destabilize the soliton.

C. Four degenerate minima: U_4

For the numerical exploration we again adopt the relevant parameters from Ref. [18]: $a = (\sqrt{3} - 1)/2$ and $b = a + 1$. This translates into $m_L = 1.793$ and $m_R = 6.692$.

In the topological sector $(-a, a)$ the background potential is symmetric under the spatial reflection $x \rightarrow -x$ as seen in the bottom left entry of Fig. 2. In this regime the

TABLE I. Numerically obtained energies from scattering solutions in the model with two degenerate minima and the parameters $a = \frac{4}{5}$ and $b = 1$. Note that the threshold is at $m_L = m_R = 3.710$. The entries E_{bind} and E_{scat} denote the bound state and continuum contributions to the VPE, i.e., the two distinct terms in Eq. (14).

Bound state energies			E_{bind}	E_{scat}	E_{vac}
0.0	2.067	3.192	3.689	−2.947	1.3722	−1.575

squared masses for the vacua are equal and consequently $q = k$ in Eq. (10). Numerically we confirm that the determinant of the scattering matrix is invariant under the translation $x \rightarrow x - x_0$ and that the VPE is independent of x_0. We present the bound state energies and the corresponding VPE for this kink solution in Table III. Besides the mandatory translational zero mode the soliton has a shape mode slightly below threshold. We show the sum of the eigenphase shifts entering this computation in the bottom left panel of Fig. 3 and read off $\delta(0) = \frac{3\pi}{2}$, confirming the existence of two bound states via Levinson's theorem.

In the case of the topological sector (a, b) we only have one bound state, the translational zero mode. Consequently $\delta(0) = \frac{\pi}{2}$ as observed in bottom right entry of Fig. 3. The binding energy is $\sum_j (E_j - m_L) = -0.896$.

In this topological sector we have $m_R(6.692) \neq m_L(1.793)$ and the existence of a threshold is also reflected by the cusp in the phase shift. More importantly, the different masses correspond to primary and secondary

TABLE II. The VPE as a function of the center of the kink x_0 in the model with three degenerate minima.

x_0	1.00	0.75	0.50	0.25	0	−0.25	−0.50	−0.75	−1.00
E_{vac}	0.254	0.215	0.176	0.138	0.0986	0.0595	0.0211	−0.0179	−0.0568

TABLE III. The bound states energies of the kink of Eq. (23) and its VPE. The last entry in parenthesis is computed via E_{vac}^S in Eq. (15).

Bound state energies	E_{bind}	E_{scat}	E_{vac}
0.0	1.644	−0.971	0.389	−0.582(0.583)

TABLE IV. The VPEs as a function of the center of the kink x_0 of the topological sector (a, b) in the four degenerate minima regime.

x_0	0.50	0.25	0	−0.25	−0.50
E_{vac}	2.628	1.869	1.111	0.348	−0.407

vacua and, as seen from Table IV, the VPE depends in the position of the soliton.

Obviously there is no lower bound to the VPE and the emergence of a secondary vacuum again causes quantum effects to destabilize the soliton.

D. Moderate differences in the curvatures

The ϕ^8 model would be a perfect sample to study the dependence of the VPE on the topological charge because the model with four minima admits soliton solutions with different charges without changing any model parameter. These are kinks that connect (a, b) and $(−a, a)$, respectively. One would simply compare the calculated VPEs. Unfortunately, the (a, b) kink induces a translational variance of the VPE and no unique value can be assigned. To nevertheless get a rough idea, we consider parameters a and b leading to $m_L = 2.0$ and $m_R = 2.5$ such that the difference in the curvatures is small to moderate. The topological charges scale as $Q_{(−a,a)}/Q_{(a,b)} = 8$ and the classical masses approximately follow that behavior $M_{(−a,a)}/M_{(a,b)} = 8.44$. Yet the $(−a, a)$ soliton is not stable energetically but topologically since $b > a$.

The VPE for this $(−a, a)$ soliton is −1.242. The translational variance of the VPE for the (a, b) soliton is listed in Table V. As expected there is only a mild (linear) dependence of the VPE on x_0 that we fit to $E_{\text{vac}} \approx \bar{E}_{\text{vac}} + \epsilon_{\text{vac}}x_0$

TABLE V. Translational variance of VPE for the (a, b) soliton for $m_L = 2$ and $m_R = 2.5$ in the model with four minima.

x_0	−1.0	0.25	0.0	0.25	1.0
E_{vac}	−0.578	−0.553	−0.550	−0.542	−0.528

with $\bar{E}_{\text{vac}} = −0.550$ and $\epsilon_{\text{vac}} = 0.025$. Assuming $\bar{E}_{\text{vac}}$ as a reasonable measure for the VPE of the (a, b) soliton we see that the VPEs in different topological sectors do not scale with the topological charge. Since this is different from the classical masses, the VPE can have significant effects when estimating the binding energies of solitons with large topological charges. To compare the VPE of the decaying soliton with that of the decay products we need to compare $8\bar{E}_{\text{vac}} \approx −4.40$ with the VPE of the $(−a, a)$ soliton and conclude that including the VPE has the potential to reduce the binding energy significantly. A scenario that was also seen for the H dibaryon in the Skyrme model [26]. In the present model the total energies depend on the particular value of the loop-counting parameter λ for which we, unfortunately, have no empirical input. Nevertheless we think that our results may alter the picture obtained for binding energies of nuclei in phenomenological soliton models [27] once the VPE is included, which is hampered by those models not being renormalizable.

E. Transition between the two and three degenerate minima models

The soliton in the model with three minima can be viewed as a limiting case of the one in the model with only two minima. As we decrease b in the U_2 model, the $(−a, a)$ configuration disintegrates into two separated $(−a, 0)$ and $(0, a)$ structures each being similar to the kinks in the model with three minima. Changing that separation translates into changing the center of the $(0, a)$ kink in the model with three minima. We hence expect that the VPE of the model with only two minima becomes large and negative as we tune b towards zero. This is exactly the behavior of the data listed in Table VI, even though there is a small increase of the VPE as we decrease b in the moderate regime. The $b \to 0$ limit of the U_2 potential takes the shape of a wide well. On the other hand, two widely separated $(−a, 0)$ and $(0, a)$ structures form a potential barrier in the U_3 model. The height of this barrier equals the depth of the well. With the no-tadpole renormalization scheme the second order contribution from the potential dominates the VPE. This second order piece is the same for the well and the barrier. Hence we can indeed expect the two scenarios in the U_2 and U_3 models to yield similar results for that limiting scenario.

VI. CONCLUSION

In this project we studied the leading (one-loop) quantum corrections to classical energies of solitons in the ϕ^8

TABLE VI. VPE as function of b in model with two minima.

b	1.0	0.7	0.5	0.2	0.1	0.08	0.07	0.06	0.05
E_{vac}	−1.574	−1.307	−1.277	−1.868	−3.162	−3.846	−4.341	−5.006	−5.947

model in one space and one time dimensions. We utilized spectral methods for this study. These methods merely require to compute the scattering data for fluctuations about the solitons. No other approximation or truncation is needed. The Born approximation enters the calculation only as a technical tool when renormalizing the ultraviolet divergences.

Central to our study has been the question of whether or not these corrections destabilize classically stable solitons. The key issue to this problem is the existence of secondary vacua. Here the ϕ^8 model is unique as it possesses these vacua, but not all soliton solutions approach these vacua at spatial infinity. Our simulations confirm the earlier conjectured picture: whenever the soliton can connect to a secondary vacuum, increasing the coverage of that vacuum (as a portion in space) reduces the quantum energy without lower bound. This signals soliton destabilization at the quantum level. This scenario is furthermore supported by computing the quantum correction in a model that only has a primary vacuum but a certain limiting choice of the model parameters approaches a model that has a secondary vacuum. The quantum correction to the energy of the soliton is also found to diverge in that limit. We stress, however, that destabilization cannot be solely attributed to the field potential but also requires a soliton configuration that connects primary and secondary vacua.

We have also obtained indications that the (one-loop) quantum correction to the energy does not scale with the topological charge, even though translational variance in the presence of secondary vacua prohibits robust conclusions. In the particle picture of soliton models the topological charge is identified as the particle number and the classical energy, which approximately scales like the charge, as the particle mass. This predestines these models to predict binding energies of compound objects, such as nuclei. Our results hence suggest that quantum corrections should not be ignored when estimating such binding energies.

ACKNOWLEDGMENTS

[1] R. Rajaraman, *Solitons and Instantons* (North-Holland, Amsterdam, 1982).

[2] N. S. Manton and P. Sutcliffe, *Topological Solitons* (Cambridge University Press, Cambridge, England, 2004).

[3] T. Vachaspati, *Kinks and Domain Walls: An Introduction to Classical and Quantum Solitons* (Cambridge University Press, Cambridge, England, 2010).

[4] A. Vilenkin and E. P. S. Shellard, *Cosmic Strings and Other Topological Defects* (Cambridge University Press, Cambridge, England, 2010).

[5] U. Schollwöck, J. Richter, D. J. J. Farnell, and R. F. Bishop, Lect. Notes Phys. **645,** 1 (2004).

[6] N. Nagaosa and Y. Tokura, Nat. Nanotechnol. **8,** 899 (2013).

[7] H. Weigel, Lect. Notes Phys. **743,** 1 (2008).

[8] G. H. Derrick, J. Math. Phys. (N.Y.) **5,** 1252 (1964).

[9] N. Graham, M. Quandt, and H. Weigel, Lect. Notes Phys. **777,** 1 (2009).

[10] A. Alonso-Izquierdo and J. Mateos Guilarte, Nucl. Phys. **B852,** 696 (2011).

[11] A. Alonso-Izquierdo and J. Mateos Guilarte, Ann. Phys. (Amsterdam) **327,** 2251 (2012).

[12] H. Weigel, Phys. Lett. B **766,** 65 (2017).

[13] H. Weigel, Adv. High Energy Phys. **2017,** 1486912 (2017).

[14] H. Weigel and N. Graham, Phys. Lett. B **783,** 434 (2018).

[15] H. Weigel, AIP Conf. Proc. **2116,** 170002 (2019).

[16] T. Romańczukiewicz, Phys. Lett. B **773,** 295 (2017).

[17] A. Khare, I. C. Christov, and A. Saxena, Phys. Rev. E **90,** 023208 (2014).

[18] V. A. Gani, V. Lensky, and M. A. Lizunova, J. High Energy Phys. 08 (2015) 147.

[19] I. C. Christov *et al.,* arXiv:2005.00154.

[20] J. S. Faulkner, J. Phys. C **10,** 4661 (1977).

[21] F. Calegero, *Variable Phase Approach to Potential Scattering* (Academic Press, New York and London, 1967).

[22] K. Kiers and W. van Dijk, J. Math. Phys. (N.Y.) **37,** 6033 (1996).

[23] N. Graham and R. L. Jaffe, Phys. Lett. B **435,** 145 (1998).

[24] G. Barton, J. Phys. A **18,** 479 (1985).

[25] N. Graham, R. L. Jaffe, M. Quandt, and H. Weigel, Ann. Phys. (Berlin) **293,** 240 (2001).

[26] F. G. Scholtz, B. Schwesinger, and H. B. Geyer, Nucl. Phys. **A561,** 542 (1993).

[27] D. T. J. Feist, P. H. C. Lau, and N. S. Manton, Phys. Rev. D **87,** 085034 (2013).